Journal of Applied Electrochemistry **32**: 977–985, 2002.

Asymmetric alumina membranes electrochemically formed in oxalic acid solution

P. BOCCHETTA[1], C. SUNSERI[1,*], A. BOTTINO[2], G. CAPANNELLI[2], G. CHIAVAROTTI[3], S. PIAZZA[1] and F. DI QUARTO[1]

[1]*Dipartimento di Ingegneria Chimica dei Processi e dei Materiali, Università di Palermo, Viale delle Scienze, 90129 Palermo, Italy*

[2]*Dipartimento di Chimica e Chimica Industriale, Università di Genova, Via Dodecanneso 31, 16146 Genova, Italy*

[3]*Becromal S.p.A, Via Ernest Rosenthal 5, 20089, Rozzano-Milano, Italy*

*(*author for correspondence, fax: +39 (0)916567280, e-mail: sunseri@dicpm.unipa.it)*

Key words: membrane preparation, microporous membranes, porous alumina, porous membranes

Abstract

Alumina membranes were fabricated by anodizing aluminium metal in 0.15 M oxalic acid. The growth kinetics of the porous layer were investigated in the temperature range −1 to 16 °C using linear potential scans up to 70 V. The faradaic efficiencies of metal oxidation and of porous layer formation, determined by applying Faraday's law, were found to be independent of both temperature and electrical charge. SEM analysis of the metal-side and solution-side surfaces revealed different morphologies. After dissolution of the barrier layer in phosphoric acid, the metal-side surface showed circular pores whose size of about 90 nm was found to be uniform and independent of temperature. The pore population was also practically independent of temperature and a value of about 4×10^{13} pores m^{-2} was determined. On the solution-side surface the presence of a deposit partially occluding the mouths of pores was observed. This coating could be removed by chemical etching in NaOH or thermal treatment at 870 °C, where decomposition of oxalate occurs. This supports the hypothesis that the deposit consists of an aluminium salt containing oxalate anions precipitated from the solution. The results show that it is possible to control the morphological characteristics of the anodic alumina membranes by careful choice of experimental conditions.

1. Introduction

In recent years alumina membranes have attracted increasing attention due to their potential use in several fields of technological interest, such as micro and ultrafiltration, catalytic reactors [1, 2], and novel electrolytes for proton exchange [3]. In comparison with membranes derived from organic polymers, alumina membranes are characterised by high stability at elevated temperature combined with chemical resistance in corrosive environments. Typically they have superior electrical and acoustic properties and wear behaviour [4]. Two common methods for producing alumina membranes are sintering, an energy-intensive method, and the more typical sol–gel method, involving the use of various solvents and acids [5]. Alternative methods are chemical vapour deposition (CVD) and anodic oxidation of aluminium [6, 7].

Among these methods the sol–gel approach is usually considered to be the most practical in making thin ceramic films with the top layer in microscale, the pore diameter in nanoscale and with narrow pore size-distribution [8, 9]. The alumina membranes made by this procedure, as well as by sintering, typically present a sponge-like morphology with high tortuosity due to pore intercrossing. In contrast, membranes from anodic oxidation of aluminium show a honeycomb structure characterised by a close-packed array of columnar hexagonal cells, each containing a central pore normal to the oxide layer surface. These features extend the use of the alumina membranes to specific applications where ordered structures are required, such as in electronic and photoelectronic devices. Typically anodic alumina membranes serve as ideal templates for the formation of nanostructured materials [10–16].

In this context the anodising process assumes a key role because the characteristics of the membranes are determined by choice of the appropriate experimental conditions. The parameters to take into account are numerous because several steps are required in order to obtain a membrane starting from aluminium metal. Initially a porous layer must be grown and its morphology depends on the solubility of the oxide in the electrolyte [17–19], as well as on the electrical parameters (for example, the applied anodizing voltage) determining the order degree of the hexagonal structure [20]. Finally, the detachment procedure of the porous layer from the residual metal and the successive etching of the surfaces can modify the membrane morphology [21].

This work is aimed at gaining a deeper insight into the electrochemical preparation of anodic alumina membranes. In particular, attention was paid to the formation of porous layers in oxalic acid using linear potential scans, in contrast with the most usual preparation procedures consisting in applying a constant current or potential [7]. To investigate the influence of temperature on the characteristics of the membranes, anodizations were performed between −1 and 16 °C. Another aspect investigated in this work was the nature of the microporous layer covering the solution-side electrode surface. The chemical nature and the mechanism of formation of this coating were investigated and experimental procedures for removing it were explored. This work shows that highly asymmetric alumina membranes, whose porosity changes throughout the thickness, could also be obtained by using an electrochemical technique and a way of controlling their porosity is suggested, which allows wide ranging application.

2. Experimental details

Discs (dia. 5 cm) were cut from 100 μm thick aluminium foils (purity 99.99%). The discs were cleaned by immersion in 1 M NaOH for 3 min, followed by rinsing in distilled water. To obtain a more ordered porous structure, the discs were electropolished at 20 V for 5 min in a $HClO_4$:C_2H_5OH solution (1:6 by volume) stirred vigorously. Electrodes were mounted on a holder in order to have a flat circular surface exposed to the solution. Anodizations were performed in 0.15 M oxalic acid by linear potential sweep at 0.2 V s^{-1} up to 70 V. A Glassman High Tension (series ER) power source and a two-electrode cell, having a Pt wire as the counter electrode, were used. The temperature of the anodizing bath was held in the interval −1 to 16 °C and was controlled within ±0.1 °C by means of a refrigerator Lauda (model RE 106). During anodization the electrolyte was stirred vigorously.

The morphology of the samples was examined at different magnifications with a Leica Stereoscan 440 scanning electron microscope (SEM). Prior to SEM examination, oxide surfaces were sputter coated with gold. To observe the pore arrangement at the metal–oxide interface, the aluminium substrate was totally dissolved in 0.1 M CuCl + 20% (w/w) HCl solution at 5 °C; then the pore bottoms were opened by chemical etching in acidic solution.

Thermal analysis of the samples was performed using a Netzch STA/409/2 thermal analysis system. Thermogravimetric analysis (TGA), differential thermogravimetric analysis (DTG), and differential thermal analysis (DTA) were performed. The oxide layers were ground into powder prior to thermal analysis, which was performed by raising the temperature at a rate of 10 °C min^{-1}.

X-ray diffraction patterns (XRD) were obtained using a Philips (model PW 1130) generator and a PW (model 1050) goniometry. The copper K_α radiation and a scanning rate of 2ϑ 1° min^{-1} were used. Measured d spacings were compared with the ASTM index values.

The weight of the aluminium discs was measured before anodization. After membrane preparation the residual aluminium was estimated by weighing the samples before and after dissolution of the metal in CuCl.

3. Results and discussion

The current–potential curves reported in Figure 1 were obtained using linear potential sweeps at 0.2 V s^{-1}; after the initial current increase the curves present a plateau, during which the growth of an aluminium oxide barrier film, more or less hydrated, occurs [22]. For longer times, an increase in the current density (c.d.) is observed, due to the pore growth by a field-assisted dissolution mechanism of the oxide at the base of the pores [23]. The shape of the curves reported in Figure 1 is dependent on temperature: as temperature increases both a decrease in the length of the plateau and an increase in current were observed. These effects are related to the kinetics of the electrode processes occurring during anodization of aluminium. In the following, the current distribution during anodization will be discussed and it will be shown that the faradaic efficiencies, determined by weight measurements, are independent of temperature. Therefore, the increase in total current with temperature, shown in Figure 1, can be justified assuming an increase in both aluminium oxidation current and electronic current, so that the faradaic efficiencies do not change.

The applied potential, U_{app}, was stopped at 70 V and this value was held for 80 min. Figure 2 shows the current behaviour at this potential: after an initial transient, the current attains an almost constant value. This steady-state current is reached when the rate of the field-enhanced dissolution of alumina at the base of the pores, (i_{diss}), equals the oxide formation rate at the

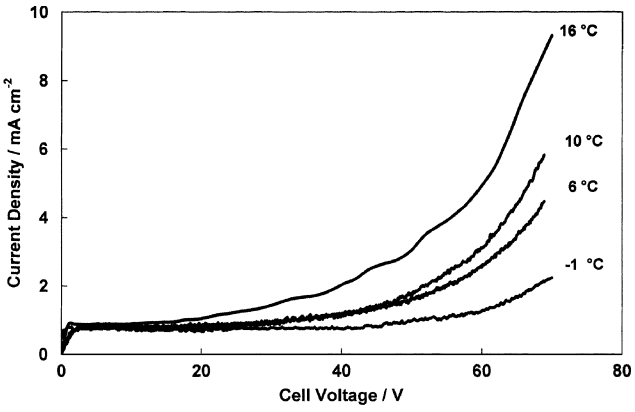

Fig. 1. Growth of an anodic oxide film on aluminium using a linear potential scan at 0.2 V s^{-1} in 0.15 M oxalic acid up to 70 V.

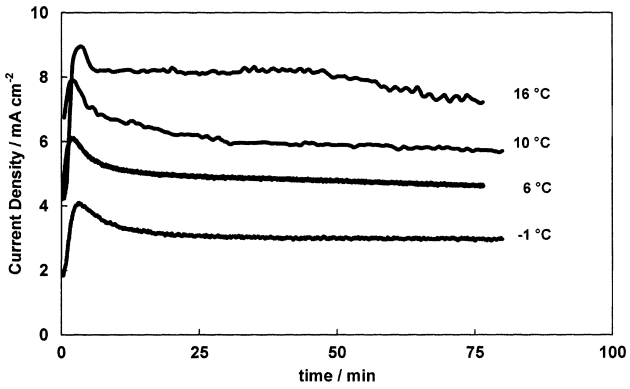

Fig. 2. Current against time curves during the growth of an anodic porous layer on aluminium at $U_{app} = 70$ V in 0.15 M oxalic acid.

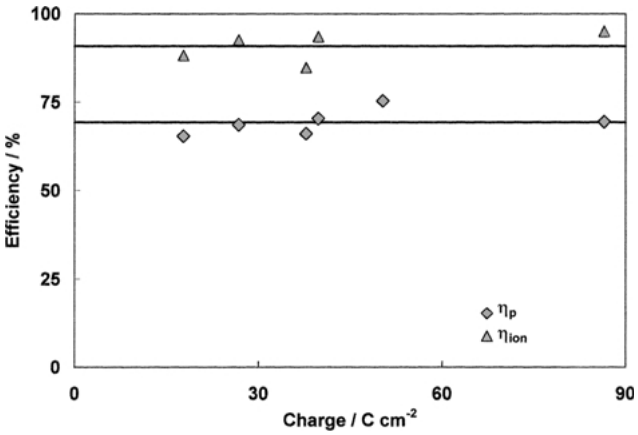

Fig. 3. Faradaic efficiencies against electric charge during anodizing of aluminium in 0.15 M oxalic acid at 70 V and 16 °C.

metal–oxide interface [24]. The current peak before reaching the steady-state conditions is typical of potentiostatic experiments [25]. Based on Figure 2, it can be assumed that the growth of the porous layer occurs under a practically constant current, increasing with bath temperature. In order to investigate the growth kinetics of the porous layer, we consider that the measured total current density, i_{tot}, is the sum of several contributions, and can be written as

$$i_{tot} = i_{ion} + i_{el} = (i_p + i_{diss}) + i_{el} \quad (1)$$

where i_{ion} is the ionic c.d., related to the amount of oxidized aluminium, i_{el} is the electronic current, due to other faradaic processes occurring at the oxide/electrolyte interface, i_p and i_{diss} are the oxide formation and metal dissolution ionic currents, respectively.

According to Faraday's law, the average i_{ion} value during the anodization process can be estimated by means of Equation 2:

$$(i_{ion})_{av} = \frac{1}{S_g} \times \frac{(m_i - m_f)_{Al}}{(M_w)_{Al}} \times \frac{zF}{\Delta t} \quad (2)$$

where S_g is the apparent surface area of the sample, m_i and m_f the initial and final weights of Al, respectively, $(M_w)_{Al}$ the molecular weight of Al, z the number of electrons exchanged in the oxidation of Al, F is Faraday's constant and Δt the elapsed time. Analogously, the average i_p value can be derived as

$$(i_p)_{av} = \frac{1}{S_g} \times \frac{m_p}{(M_w)_{Al_2O_3}} \times \frac{zF}{\Delta t} \quad (3)$$

where m_p is the weight of the porous layer and $(M_w)_{Al_2O_3}$ the molecular weight of Al_2O_3. From Equations 1–3, the average dissolution current, $(i_d)_{av}$, can be calculated as

$$(i_d)_{av} = (i_{ion})_{av} - (i_p)_{av} \quad (4)$$

For determining the current distribution from the measured steady-state total current density, we have estimated the following faradaic efficiencies:

$$\eta_{ion} = i_{ion}/i_{tot} \quad \text{and} \quad \eta_p = i_p/i_{tot} \quad (5)$$

as functions of temperature and electric charge.

Both faradaic efficiencies, calculated at each temperature, were found to be practically independent of the electric charge, as shown in Figure 3, where the results at 16 °C are reported. As for the dependence on temperature, the efficiency values, averaged over several runs, are reported in Table 1: the η values are rather similar, with a maximum variation between different temperatures within 10%. Taking into account the typical uncertainty of a weight measurement, such a variation appears acceptable. Therefore we assumed both η_{ion} and η_p independent of temperature, and the average values of 90.97% for η_{ion} and 71.7% for η_p were used to determine the current distribution during anodization. An alternative procedure, based on the best fitting of the faradaic efficiency vs temperature, gives 89.6% for η_{ion} and 72% for η_p which are very close to the previous ones. These values of η_p are comparable with the 67% determined by Siejka et al. [25] for the anodization of aluminium in 15% H_2SO_4, whilst the independence of the faradaic efficiencies from the temperature, reported here, is at variance with other literature data [26]. This discrepancy can be attributed to the different nature of the electrolyte used (phosphoric acid) and to the different temperature interval exploited (20–30 °C) in [26]. Such conditions are more aggressive for aluminium oxide and could determine a different electrochemical behaviour, producing a different temperature dependence of the faradaic efficiencies.

Table 1. Faradaic efficiencies at different temperatures for the anodizing process of aluminium in 0.15 M oxalic acid at 70 V

T/°C	η ion,av/%	η p,av/%
−1	87.71	70.00
6	96.39	76.49
10	88.97	71.05
16	90.85	69.26

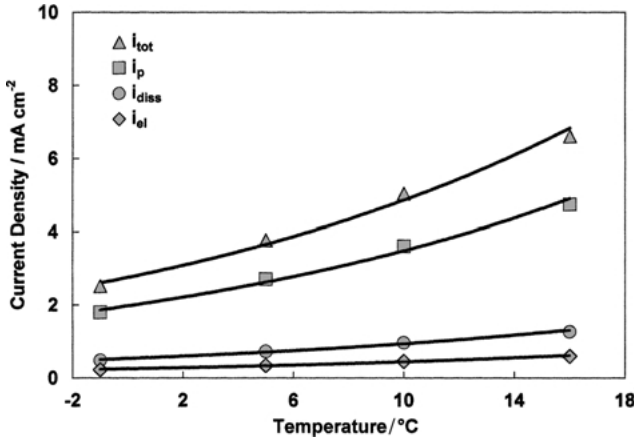

Fig. 4. Current distribution against temperature for an anodic oxide film growing on aluminium in 0.15 M oxalic acid.

Figure 4 shows curves of i_p, i_{diss}, i_{el} and i_{tot} against T, determined according to Equations 1–5. It is evident that the ionic current, i_{ion}, estimated as the sum of i_p and i_{diss}, changes from 2.29 mA cm^{-2} at -1 °C to 6.00 mA cm^{-2} at 16 °C. Both the dissolution and the electronic current are very low, reaching a maximum value of 1.27 mA cm^{-2} and 0.6 mA cm^{-2}, respectively, at 16 °C. The electronic current is originated by the oxygen evolution side-reaction, whilst the dissolution current is related to the electric field strength at the oxide/electrolyte interface.

The thickness of the porous layer was found to increase linearly with electric charge, as shown by Figure 5, where it is evident that saturation conditions are not reached in the interval of electric charge explored. The Figure also shows that on changing temperature from -1 °C to 16 °C the slopes of the straight-lines vary from 34 nm cm^2 C^{-1} to 32 nm cm^2 C^{-1}; this confirms the independence of the faradaic efficiencies from temperature, previously noted. From a practical point of view, these findings indicate that it is advantageous to anodise aluminium at the highest temperature to accelerate the growth of the porous layer. On the basis of the gravimetric results, the energy consumption necessary to produce 1 μg of membrane in 0.15 M oxalic acid is about 0.59 J μg^{-1}, in the temperature range -1 to 16 °C, whilst the aluminium consumed is 0.72 μg Al (μg membrane)$^{-1}$.

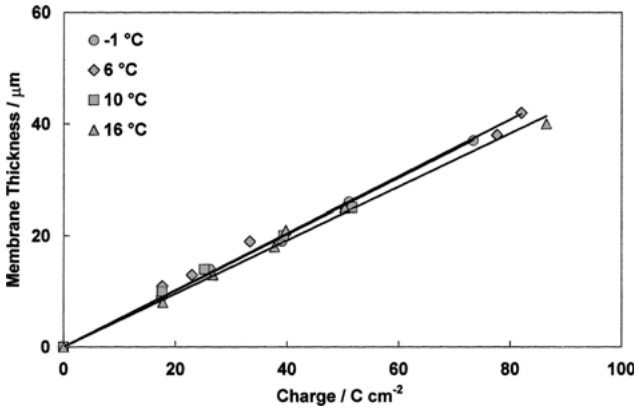

Fig. 5. Thickness of alumina membranes, fabricated at different temperatures in 0.15 M oxalic acid at 70 V, as a function of electric charge.

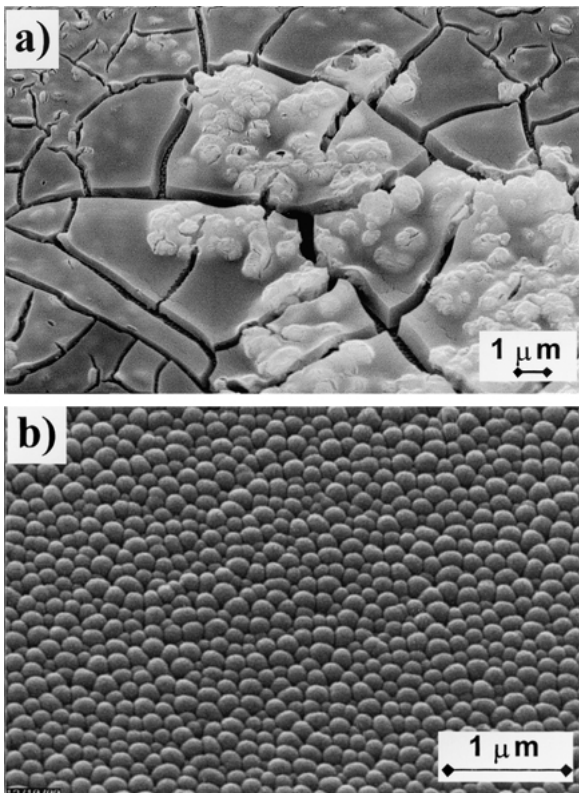

Fig. 6. SEM picture of the metal-side surface of an alumina membrane prepared in 0.15 M oxalic acid at 70 V and 16 °C. (a) Before dissolution of the residual aluminium metal. (b) Final morphology after the complete removal of the metal in 0.1 M CuCl.

After anodization the residual aluminium was removed by chemical etching. The morphology of samples prepared at 70 V in 0.15 M $(COOH)_2$ at 16 °C during the dissolution process is shown in Figure 6(a), where the presence of fractured structures above the anodic alumina oxide is evident. In some points of the micrograph it is also possible to detect the morphology of the underlying layer. After dissolution of the metal was completed and the sample was carefully washed with distilled water, the morphology of the bottom of the porous layer appears as in Figure 6(b), where a rather uniform distribution of spheroidal matter is evident. The cross-section of Figure 7 shows that spheres of Figure 6(b) are really hemispheres corresponding to the bottom of the pores.

Usually the porosity of the sample is determined by analysing this surface rather than the solution-side surface, because dissolution of the oxide at the interface with the solution during the anodization can cause enlargement of the pore mouths, with consequent errors in the determination of pore size. Some authors have estimated this error to be of the order of 20% for membranes prepared in 0.3 M $(COOH)_2$ at 40 V and 1 °C [20]. It is difficult to generalize this estimate because

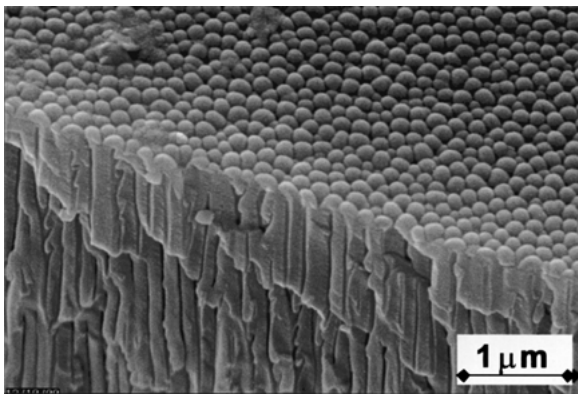

Fig. 7. Section-view for the sample of Figure 6(b).

it depends on the immersion time of the sample, which was 2–4 days in [20] and in the order of few hours for our specimens. In our experiments, another factor inhibiting the analysis of the solution-side image for determining the porosity is the formation of a layer partially covering the pores during anodization. As discussed below, this layer can be removed by immersion in NaOH solution but this procedure can sharply modify the pore size.

The porosity of the membranes, prepared in 0.15 M $(COOH)_2$ is shown in Figure 8 as a function of temperature: a slight decrease in porosity as the temperature of the bath increases from -1 to 16 °C is evident. This finding was confirmed by comparing the porosity data derived from SEM analysis with those obtained from gravimetric measurements. In the former case, the values of porosity were obtained according to the following equation:

$$\text{Porosity} = \frac{S_{\text{pore}}}{S_{\text{g}}} = \frac{S_{\text{g}} - S_{\text{ox}}}{S_{\text{g}}} = 1 - \frac{m_{\text{p}}}{\rho h S_{\text{g}}} \tag{6}$$

where S_{pore} is the total surface of pores, S_{ox} is the oxide surface, h is the thickness of the porous layer and ρ is the density of alumina. Once the geometric electrode area, S_{g} was known, the best fit was performed by using the experimental values of both m_{p} (obtained by gravimetric measurements) and h (obtained by thickness measurements). The only adjustable parameter was ρ and the best fitting was found for a value of 3.25 g cm^{-3}, which agrees with 3.2 g cm^{-3} reported by Liu et al. for amorphous Al_2O_3 barrier films [27]. The high sensitivity of the fitting curve to the density value assumed for alumina is shown in Figure 9, where it is evident that a density variation of $\pm 5\%$, with respect to the best fitting value of 3.25 g cm^{-3} gives a porosity variation of about $\pm 15\%$. Taking into account that the two procedures used for determining the porosity values are independent of each other, the good fitting confirms the reliability of the data obtained by SEM analysis. To explain the slight decrease in porosity with increasing temperature, we consider the dependence of both pore density and pore size on this parameter. Such a dependence is reported in Table 2, where it is shown that pore density decreases steadily from -1 to 16 °C, whilst pore size is almost constant. Therefore, the variation of porosity can be attributed to the variation of pore density. The uniformity of pore size and its independence of bath temperature is further supported by Figure 10, showing that the distribution curves of pore diameter for three different temperatures are quite narrow and practically coincident.

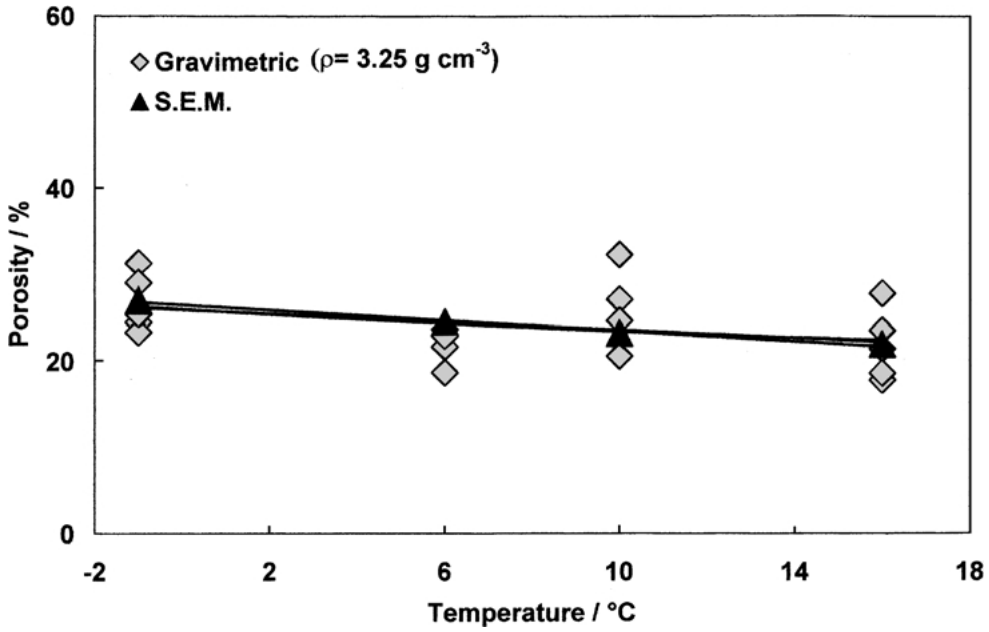

Fig. 8. Porosity against temperature for alumina membranes fabricated in 0.15 M oxalic acid at 70 V. Gravimetric porosity was determined by a trial and error method, using the density of the porous layer as adjustable parameter. Best value was 3.25 g cm^{-3}.

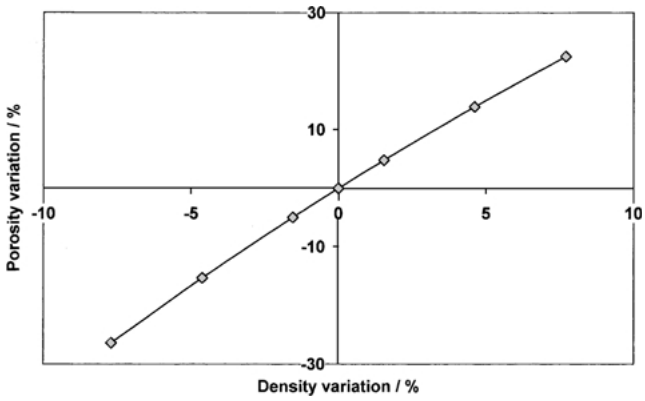

Fig. 9. Percentage porosity variation against percentage density variation with respect to the best fitting value of Figure 8.

Table 2. Pore size and density for alumina membranes fabricated at 70 V in 0.15 M oxalic acid at different temperatures

T/°C	Porosity/%	Pore density /pores m^{-2}	Pore size/nm
−1	26.9	4.20×10^{13}	90.40
6	24.47	3.90×10^{13}	89.45
10	23.2	3.78×10^{13}	88.40
16	21.9	3.65×10^{13}	87.38

To open the pores at the metal-side surface, the alumina barrier layer was dissolved by chemical etching in acidic or alkaline bath. The dependence of morphology on the composition of the etching solution is shown in Figure 11 (a,b): in (b) pore walls are thinner with frequent breakage of pores, whereas in (a) pores more uniform in size, having thicker walls, were obtained. These findings could suggest a way of controlling, to a small extent, porosity of membranes, by changing the dissolution procedure of the barrier layer. Another way to detach the porous layer from the underlying metal consists in a step-by-step reduction of the applied potential, starting from the anodising potential down to 0 V [7]. During each step, each pore generates two new smaller pores penetrating the barrier layer down to the metal surface, so that a microporous layer, consisting of pores with decreasing size, is obtained; the thickness of the microporous layer is equal to that of the barrier layer [21].

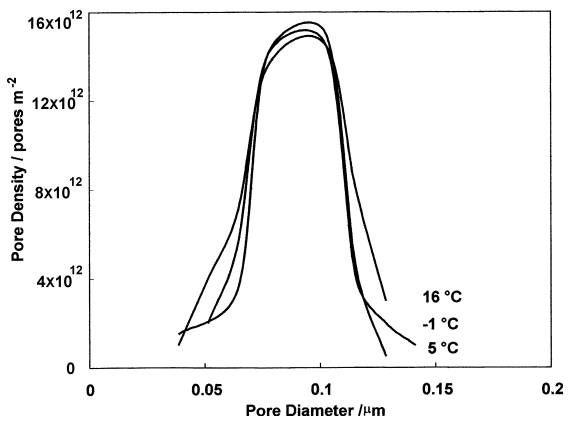

Fig. 10. Distribution curves of pore diameter for alumina membranes fabricated in 0.15 M oxalic acid at different temperatures.

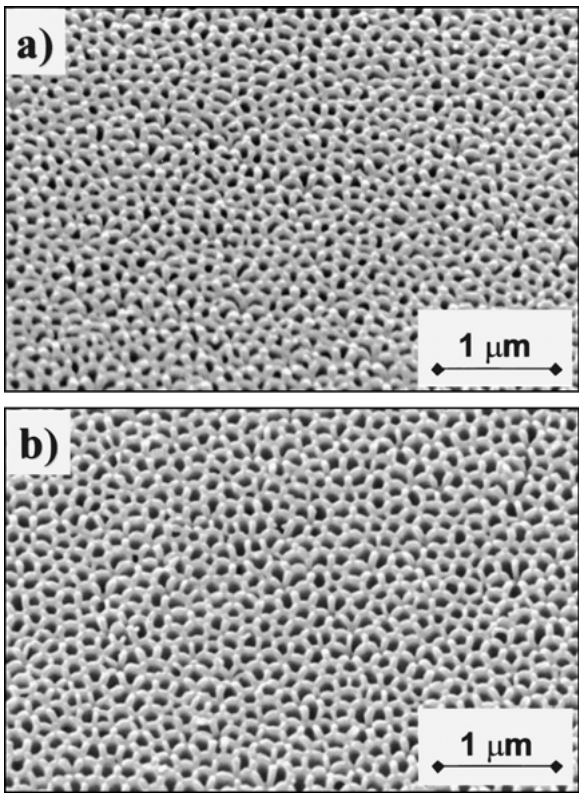

Fig. 11. Morphology of the metal-side surface of a membrane after removal of the barrier layer in: (a) acidic solutions; (b) alkaline solutions. Anodic porous layer was grown in 0.15 M oxalic acid at 70 V and 16 °C.

Soon after preparation, alumina membranes were also characterized by TGA and XRD analysis. TGA was performed on samples prepared at all temperatures in the range −1 to 16 °C. Only one peak, at around 870 °C, is observed in the DTG analysis. The corresponding weight loss is about 6%, while the DTA indicates that an exothermic reaction occurs at the same temperature. Table 3 gives the weight loss for different initial weights of membranes prepared at 16 °C: in all cases the weight loss is about 6%, and is independent of the anodizing process duration. This value is close to the 8% reported in [27]. Both weight loss and exothermic peak can be attributed to the pyrolysis of oxalate anions, according to reference [13] cited in [27], reporting a decomposition temperature of 915 °C for oxalate anions in anodic aluminium oxide grown in oxalic acid solution. This temperature is fairly close to the 870 °C determined by DTG in the present work. The occurrence of a crystallization process in this temperature range must also be taken into account: other authors

Table 3. Weight loss, determined from thermal analysis, for membranes prepared in 0.15 M oxalic acid at 70 V and 16 °C

Initial weight/mg	Weight loss/%
43.9	6.38
155.4	5.98
180.5	6.15
246.7	6.15

[28] attribute both the exothermic peak and the weight loss observed at 840 °C to the crystallization of membranes prepared in oxalic acid. The discrepancy existing in the literature in the interpretation of thermal analysis on anodic alumina membranes is evident: for some authors only a crystallization process with weight loss occurs at 840 °C [28], while other authors report only decomposition of organic matter incorporated into the anodic film [27]. To investigate this aspect, the anodic alumina membranes were also analysed by XRD. Freshly prepared membranes were found to be amorphous, while after thermal treatment alumina crystallizes. Figure 12 shows typical X-ray diffraction patterns for a membrane prepared at 16 °C and held in air at 870 °C for 7 h. The identification of the peaks [29] reveals that alumina crystallizes in the form of δ-Al_2O_3 and ϑ-Al_2O_3. The aforementioned discrepancy in the interpretation of the results of thermal analysis can be explained on the basis of this result, indicating that in the temperature range between 840 and 915 °C both crystallization of anodic alumina and decomposition of the oxalate anions into the porous layer occur.

This last result helps understand the morphology observed for the solution-side surface of the porous layers formed in 0.15 M $(COOH)_2$ at any investigated temperature from −1 to 16 °C. Figure 13(a) shows a surface with a uniform microporosity having irregular shape, while the section view of Figure 13(b) shows clearly that the microporosity is due to a thin layer occluding the pore mouths. This surface morphology can be modified by different treatments. Figure 14 shows the effect of etching in alkaline solution. In particular, Figure 14(a) shows the surface while the chemical treatment is in progress; two zones can be distinguished: the first on the left corner, is the practically unmodified surface, whereas the other displays the appearance of pore mouths. Figure 14(b) is the SEM picture of the same surface after treatment in NaOH solution: a porous surface is fully developed, with pores prevalently circular and uniformly distributed along the surface. It can also be observed that at some points pore walls dissolve leading to the formation of new irregularly shaped pores. This effect is typical of the treatment of the porous alumina surface in NaOH, as previously pointed out. Figure 15 shows that the morphology of the solution-side surface of freshly formed porous layers can be also modified by heating at 870 °C for 7 h. After such a treatment, the presence on the surface of circular pores is evident. These results support the hypothesis that the microporous layer obstructing the pore mouths is formed owing to precipitation from the solution of an aluminium salt containing oxalate anions; this layer dissolves in alkaline solution or decomposes under heating at 870 °C, according to the TGA results. Despite the fact that deposits obtained by precipitation are usually irregular, in the present case a uniform and flat surface deposit layer was obtained with deposition under vigorous agitation.

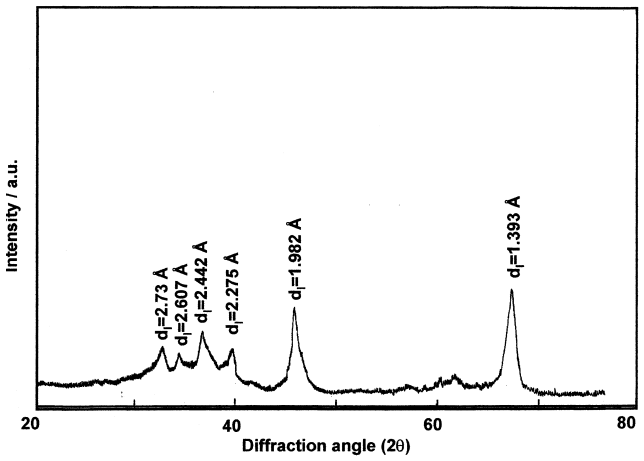

Fig. 12. X-ray diffraction patterns for an anodic alumina membrane prepared in 0.15 M oxalic acid at 70 V and 16 °C, and heated at 870 °C in air for 7 h.

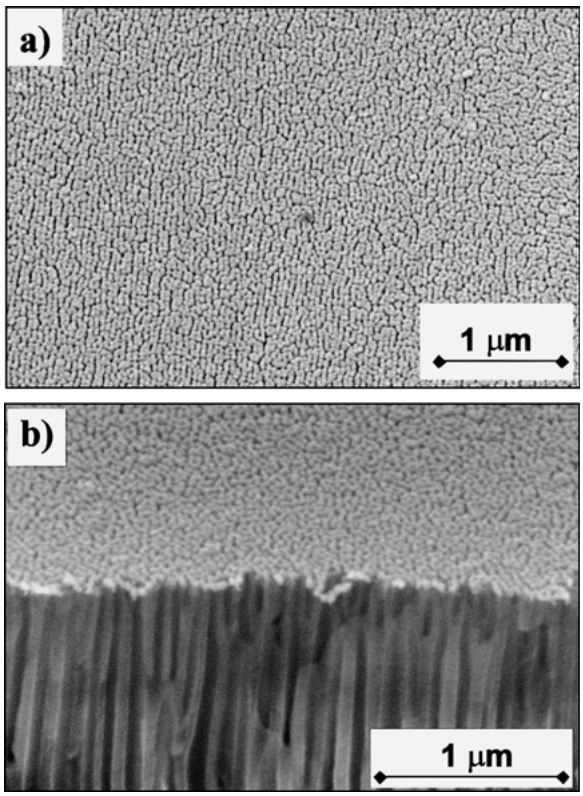

Fig. 13. Morphology of the solution-side surface at the end of the anodising process of aluminium in 0.15 M oxalic acid at 70 V and 16 °C. (a) Top view; (b) section view.

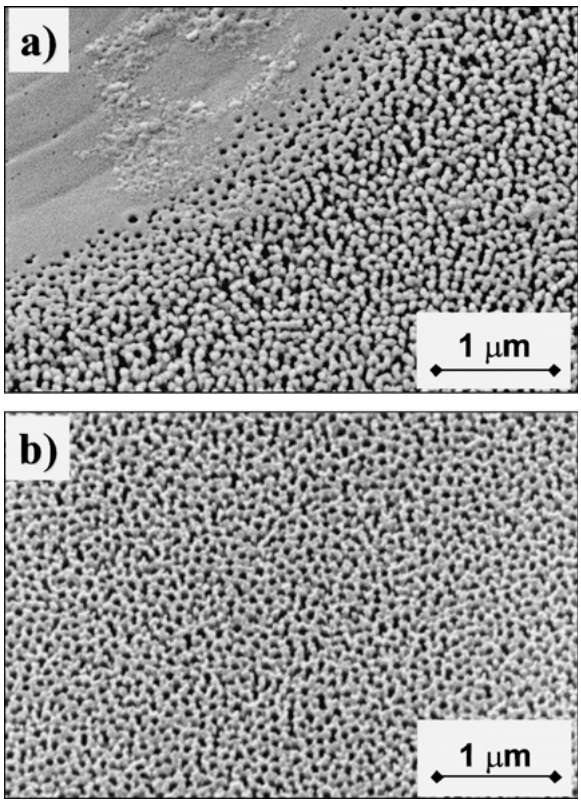

Fig. 14. SEM pictures of the surface of Figure 11 during a chemical treatment in 1 M NaOH for 2 min. (a) Initial stage of treatment; (b) final morphology.

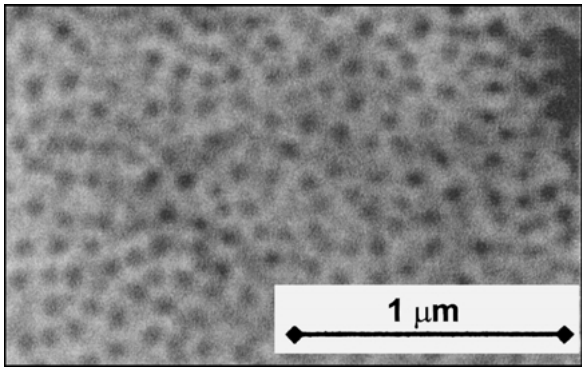

Fig. 15. Morphology of the solution-side surface for a membrane prepared in 0.15 M oxalic acid at 70 V and 16 °C, and held in air at 870 °C for 7 h.

4. Summary

The fabrication of anodic membranes in 0.15 M oxalic acid starting from aluminium metal was investigated. The anodising process was performed in the range −1 to 16 °C using linear potential scans up to 70 V. The faradaic efficiencies of the metal oxidation process, η_{ion}, and of the porous layer formation, η_p, were determined by applying Faraday's law. They were found to be independent of both electrical charge and temperature, with average values of 90.97% for η_{ion} and 71.7% for η_p.

The morphological characterization, performed by SEM, revealed that, after anodization, highly asymmetric membranes are formed. After dissolution of the residual aluminium, the pore bottom shows a typical morphology, with hemispheres uniformly distributed on the surface. A uniform pore size of about 90 nm was found, independent of temperature. The pore density was also practically independent of temperature and a value of about 4×10^{13} pores m^{-2} was determined. The bottom of the pores can be dissolved by etching in acidic or alkaline solutions.

On the solution-side surface of the membrane a different morphology was observed, due to a deposit layer partially occluding pore mouths. On the basis of the chemical behaviour and thermal analysis this layer was identified as an aluminium salt containing oxalate anions, formed by precipitation from the solution. This layer can be removed by chemical etching or by thermal treatment at 870 °C in air, where crystallization of the amorphous alumina formed anodically also occurs.

The results of this work show the possibility of fabricating alumina membranes with different morphology by varying the experimental conditions, so that membranes for specific applications might be tailored. For this purpose further investigations, aimed at gaining deeper insight into the influence of the preparation procedures on membrane properties are necessary.

Acknowledgement

The authors gratefully acknowledge financial support from MURST – Cofin 1999 and Becromal S.p.A., Milan.

References

1. J. Corona and J. Santamaria, *Catal. Today* **51** (1999) 377.
2. A. Julbe, D. Farrugsen and C. Guizard, *J. Membr. Sci.* **181** (2001) 3.
3. F.M. Vichi, M.T. Colomer and M.A. Anderson, *Electrochem. Solid State Lett.* **2** (1999) 313.
4. N. Wara Androff, F. Francis and B.V. Velamakanni, *AIChE J.* **43** (11A) (1997) 2878.
5. Li Shi and N.-B. Wong, *J. Mater. Res.* **14** (1999) 3599.
6. M. Pan, C. Cooper, Y.S. Lin and G.Y. Meng, *J. Membr. Sci.* **158** (1999) 235.
7. R.C. Furneaux, W.R. Rigby and A.P. Davidson, *Nature* **337** (1989) 147.
8. A. Larbot, J.P. Fabre, C. Guizard and L. Cot, *J. Membr. Sci.* **39** (1988) 302.
9. T. Okubo, M. Watanabe, K. Kusakabe and S. Morooka, *J. Membr. Sci.* **25** (1990) 4822.
10. H. Masuda and K. Fukuda, *Science* **268** (1995) 1466.
11. G. Che, B.B. Lakshmi, Ellen R. Fisher and C.R. Martin, *Nature* **393** (1988) 346.
12. T.A. Hanaoka, A. Heilmann, M. Kroll, H.P. Kormann, T. Sawitowski, G. Schmid, P. Jutzi, A. Klipp, U. Kreibig and R. Neuendorf, *Appl. Organometal. Chem.* **12** (1998) 367.
13. G. Shi, C.M. Mo, W.L. Cai and L.D. Zhang, *Solid State Commun.* **115** (2000) 253.

14. N.V. Gaponenko, O.V. Sergeev, E.A. Stepanova, V.M. Parkun, A.V. Mudry, H. Gnaser, J. Misiewicz, R. Heiderhoff, L.J. Balk and G.E. Thompson, *J. Electrochem. Soc.* **148** (2001) H13.
15. F. Muller, A-D. Muller, M. Kroll and G. Schmid, *Appl. Surf. Sci.* **171** (2001) 125.
16. Y. Lei, L.D. Zhang, G.W. Meng, G.H. Li, X.Y. Zhang, C.H. Liang, W. Chen and S.X. Wang, *Appl. Phys. Lett.* **78** (2001) 1.
17. J.W. Diggle, T.C. Downie and C.W. Goulding, *Chem. Rev.* **69** (1969) 370.
18. Y. Xu, G.E. Thompson and G.C. Wood, *Electrochim. Acta* **27** (1982) 1623.
19. G.E. Thompson, Y. Xu, P. Skeldon, K. Shimizu, S.H. Han and G.C. Wood, *Phil. Mag.* **55** (1987) 651.
20. O. Jessensky, F. Muller and U. Gosele, *J. Electrochem. Soc.* **145** (1998) 3735.
21. P. Bocchetta, C. Sunseri, E. Drioli, A. Regina, S. Piazza and F. Di Quarto, in preparation.
22. F. Di Quarto, C. Gentile, S. Piazza and C. Sunseri, *J. Electrochem. Soc.* **138** (1991) 1856.
23. A. Despic and V.P. Parkhutick, *in* J.O.'M Bockris, R.E. White and B.E. Conway (Ed), *Modern Aspects of Electrochemistry*, No. 20, (Plenum Press, New York, 1989) p. 401.
24. J.P. O'Sullivan and G.C. Wood, *Proc. R. Soc. Lond., Ser. A* **317** (1970) 511.
25. J. Siejka and C. Ortega, *J. Electrochem. Soc.* **124** (1977) 883.
26. A.T. Shawaqfeh and R.E. Baltus, *J. Electrochem. Soc.* **145** (1998) 2699.
27. Y. Liu, R.S. Alwitt and K. Shimizu, *J. Electrochem Soc.* **147** (2000) 1382.
28. C.-W. Lee, H.-S. Kang, Y.-H. Chang and Y.-M. Hahm, *Korean J. Chem. Eng.* **17** (2000) 266.
29. JCPDS International Centre for Diffraction Data: file No. 16-394 (Philadelphia, 1974); file No. 23-1009 (Philadelphia, 1983).